Antimicrobial activity of graphene oxide-metal hybrids

K. A. Whitehead,[a*] M. Vaidya[a], C. M. Liauw[a], D. A. C. Brownson[b], P. Ramalingam[b,c] J Kamieniak,[b] S. J. Rowley-Neale[b], L. A. Tetlow[a], J. S. T. Wilson-Nieuwenhuis [a], D. Brown[a], A. J. McBain[d], J. Kulandaivel [c] and C. E. Banks[a,b]

[a] School of Healthcare Science, Manchester Metropolitan University, Chester Street, Manchester M1 5GD UK

[b] Faculty of Science and Engineering, Manchester Metropolitan University, Manchester, Chester Street, M1 5GD UK

[c] Centre for Nanoscience and Nanotechnology, School of Physics, Bharathidasan University, Tamil Nadu, 620024, India

[d] Faculty of Biology, Medicine and Health, University of Manchester, Manchester, M13 9PT UK

Abstract

With resistant bacteria on the increase, there is a need for new combinations of antimicrobials / biocidal agents to help control the transmission of such microorganisms. Particulate forms of graphite, graphene oxide (GO) and metal-hybrid compounds (silver-graphene oxide (AgGO) and zinc oxide graphene oxide (ZnOGO)) were fabricated and characterised. X-Ray diffraction and Diffuse Reflectance Infrared Fourier Transform Spectroscopy demonstrated the composition of the compounds. Scanning Electron Microscopy and Energy Dispersive X-Ray Spectroscopy determined the compounds were heterogeneous and irregular in shape and size and that the level of silver in the AgGO sample was 57.9 wt.% and the ZnOGO contained 72.65 wt. % zinc. The compounds were tested for their antimicrobial activity against four prominent bacteria; *Escherichia coli, Staphylococcus aureus, Enterococcus faecium* and *Klebsiella*

pneumoniae. AgGO was the most effective antimicrobial (Minimum inhibitory concentration *E. coli / Enterococcus faecium* 0.125 mg mL^{-1}*; S. aureus / K. pneumoniae* 0.25 mg mL^{-1}). The addition of Ag enhanced the activity of GO against the bacteria tested, including the generally recalcitrant *K. pneumoniae* and *Enterococcus faecium*. These findings demonstrated that GO-metal hybrids have the potential to be utilised as novel antimicrobials or biocides in liquid formulations, biomaterials or coatings for use in the treatment of wounds where medically relevant bacteria are becoming increasingly resistant.

Keyword: Antimicrobials; graphene oxide, biocide; ESKAPE; nano / micro particles; pathogens

1. Introduction

Concerns about bacterial resistance from community-acquired and food-borne pathogens has been growing for a number of years at both national and international levels. Several Gram-positive and Gram-negative bacteria including *Escherichia coli, Klebsiella pneumoniae, Enterococcus faecium* and *Staphylococcus aureus* are currently considered as emergent global pathogens, which pose a huge global health problem (Boucher et al., 2009).

Metals have been used for decades to treat various infectious diseases, and their antimicrobial efficacies are now being re-evaluated owing to the emergence of resilient pathogens. A particular interest has emerged particularly in the use of these compounds for topical / therapeutic use as well as for disinfection to prevent the adhesion and transmission of bacterial species. Silver is one of the most widely investigated metals for antimicrobial applications, and is being used in a number of medical purposes including catheters, biomaterials and wound dressings. Zinc oxide (ZnO) is used in such applications as food packaging (Tayel et al., 2011), textiles (Velmurugan et al., 2016), as antimicrobials (Deokar et al., 2016), and in wound dressings (Chaturvedi et al., 2016). Nanoparticles are interesting in that they can be synthesized with a high surface area to volume ratio and with unusual morphologies that contain sharp

edges and corners. Graphite and the graphene derivatives have traditionally been used in electrochemistry, from applications in energy technologies, such as batteries and fuel cells and they have also been used in an array of functional composites (Unwin, et al., 2016). Work has recently suggested that the graphene family of compounds also possess antimicrobial properties (Liu et al., 2011; Wang et al., 2012). By combining the antimicrobial activity of metals together with the physical effect of GO on the bacterial cell walls, it may be hypothesised that the antimicrobial activity of graphene products may be increased.

A number of disinfectants and antiseptics have been reported to be showing signs of becoming less effective so there is a need for the development of novel microbicides due to the current limitations (Russel and Chopra, 1990; Jennings et al 2015). Transmission and infection problems due to bacterial adhesion to surfaces can be mitigated in part by the development of alternative antimicrobial sources / biocides. The aim of this work was to determine if metal-GO hybrid compounds demonstrated increased antimicrobial efficacy compared to graphite and GO, against a range of bacteria. The development of such alternative antimicrobial actives may prove beneficial for use in such formulations such as biocidal, disinfecting or topical antimicrobials or cleaning agents or for incorporation into biomaterial coatings.

2. Materials and Methods

2.1 Synthesis of compounds and characterisation

For the synthesis of the compounds, all chemicals (analytical grade or higher) were used as received from Sigma-Aldrich (UK) without any further purification and all solutions were prepared with deionised water of resistivity not less than 18.2 MΩ cm. Synthetic graphite powder was commercially obtained from Gwent Group (Pontypool, UK).

Graphene oxide (GO) was synthesized by the Hummers method *via* the oxidation of synthetic graphite (Hummers Jr and Offeman, 1958). Graphite flakes (5 g) and $NaNO_3$ (2.5 g) were combined in 115 mL of H_2SO_4 (conc.) and stirred for 30 min. Whilst kept in an ice bath (<5

°C), $KMnO_4$ (15.0 g) was gradually added to the suspension and the rate of addition was controlled to keep the reaction temperature below 15 °C. The mixture was heated to 35 °C for a 30 min period and underwent continuous stirring producing a brown paste. A further dilution was made by adding 250 ml of water to the mixture and the temperature was increased to 70 °C for 15 min. The resultant mixture was diluted by adding H_2O until a final volume of 1 L was obtained. Finally, the solution was treated with 15 mL of H_2O_2 (30 % w/w) to terminate the reaction, at which stage the solution became yellow in appearance. For purification, the mixture was filtrated and the obtained solid was washed thoroughly with Milli Q water several times in order to avoid sulphate contamination. After purification, the powder was dried at 60 °C during 48 h.

In the preparation of the AgGO, a sonochemical reduction method was utilised (Anandan and Muthukumaran, 2015). Following preparation of the GO, 0.5 g was added to 150 mL of ethylene glycol and sonicated for 30 min. In a separate vesicle, 1.0 g of silver nitrate was added to 20 mL of ethylene glycol and sonicated for 30 min. The silver nitrate dispersion was added drop-wise to the GO solution whilst undergoing sonication for 30 min to produce a homogeneous mixture. Finally, 50 mL of 0.1 M $NaBH_4$ was added to the resultant AgGO mixture and a further 30 min of sonication was performed. The product was purified with repeated steps of H_2O and ethanol washing, after which the solution was dried at 50 °C.

The ZnOGO was fabricated by dissolving 5.0 g GO in 200 mL of N, N,-dimethylformamide (DMF), along with 20 ml of 1 M zinc acetate dihydrate (pH of 6.5). The homogeneous solution was heated to 60 °C and was stirred continuously for 120 min, after which the solution was heated to 250 °C. Following solvent evaporation, partial ZnO / ZnOHGO was produced. The resulting dried product was collected and ground in an agate mortar prior to being annealed at 450 °C for 120 min within atmospheric conditions to obtain the final ZnOGO product (Liu et al., 2012).

2.1.1 Preparation of compounds for testing

For the analysis of the fabricated compounds, 20 mg of each test compound was added to 20 mL of sterile distilled water. The samples were vortexed for 10 s and immediately 10 µL of prepared sample was pipetted onto a 10 mm x 10 mm polished silicon wafer (Montco Silicon Technologies, USA) and air dried for 30 min. The samples were stored at room temperature, in desiccators until use.

2.1.2 X-Ray Diffraction (XRD)

In order to identify the crystal phase of the compounds, X-Ray Diffraction (XRD) was performed using a PANalytical X'pert powder diffraction platform. Nickel filtered copper K_α radiation (l = 1.54 Å) was used, with an anode voltage of 40 kV an anode current of 30 mA. A reflection transmission spinner stage (15 rpm) was implemented to hold the powder samples. The XRD parameters were step size: 0.13; sample: powder; slit (antiscatter) size: 1/4°. The 2q range was set between 10° and 100°, in correspondence with literature ranges associated with the characterised samples (Li et al., 2007; Zhou et al., 2007; Kumar et al., 2013; Chowdhuri et al., 2015; Liu et al., 2016). Additionally, to ensure well-defined peaks, an exposure of 50 s per 2q step was implemented.

2.1.3 Diffuse Reflectance Infrared Fourier Transform Spectroscopy (DRIFTS)

Diffuse Reflectance Fourier Transform Infrared Spectroscopy (DRIFTS) was carried out using a Spectra-Tech DRIFTS cell fitted in a Thermo – Nicolet Nexus FTIR spectrophotometer. The instrument was thoroughly purged (30 L / min) with CO_2 and water-free air, produced using a Balaston purge gas generator. All samples were diluted to ca. 5 % wt. in finely ground KBr (Sigma, UK). The samples were used as received, with no further grinding. The sample was folded into the pre-ground KBr using a micro-spatula. The micro-sampling cup was over-filled slightly and the cup dropped from a height of 1 cm onto the bench in order to shake off the excess mixture whilst at the same time, produce a slightly domed and naturally randomised,

surface of KBr diluted sample. The same batch of ground KBr was used as the background. The background and sample spectra were made up of 164 scans with resolution set to 4 cm^{-1}. As the sample was diluted with KBr there were no specular reflection components so a blocker was not used. Spectra were plotted in absorbance (Liauw, 2003).

2.1.4 Scanning Electron Microscopy (SEM) and Energy Dispersive X-Ray Spectroscopy (EDX)

In order to determine the shape, size and atomic elemental weight of the compounds, the samples were fixed to stubs using carbon tabs (Agar, UK). Scanning Electron Microscopy (Carl Zeiss Ltd.) was carried out using a Supra 40VP SEM with SmartSEM software. Energy Dispersive X-Ray (EDAX Inc.) was carried out using an Apollo 40 SDD system with Genesis software.

2.2 Microbiology and antibacterial testing

2.2.1 Stock cultures of bacteria

In preparation for the antimicrobial assays, stock cultures of *S. aureus* NCTC 4137, *K. pneumoniae* NCTC 9633 or *E. coli* NCTC 10418 were inoculated onto nutrient agar (NA) or nutrient broth (NB) and incubated at 37 °C for 24 h. Stock cultures of *Enterococcus faecium* NCTC 7171 were cultured onto Columbia blood agar with horse blood in a 5 %, Brain heart infusion agar (BHIA) (Oxoid, UK) or brain heart infusion broth (BIHB) and incubated in 5 % CO_2 for 24 h at 37 °C. All medias were obtained from Oxoid (UK).

2.2.2 Preparation of microbiological cultures

Ten millilitres of appropriate broth was inoculated with a single colony of bacteria and incubated overnight according to the above conditions. Following incubation, cells were harvested at 567 × *g* for 10 min and washed once, re-suspended in sterile distilled water, vortexed for 30 s, and then centrifuged again at 567 × *g* for 10 min. The inocula were examined in a spectrophotometer at 540 nm and compared against a blank of sterile distilled water to determine their optical density. They were then diluted accordingly and quantified using serial

dilutions. The cell concentrations corresponded to; *E. coli* 4.20×10^8, *S. aureus* 1.30×10^8, *Enterococcus faecium* 3.95×10^8 and *K. pneumoniae* 2.82×10^8 colony forming units per mL (CFU / mL).

2.2.3 Zones of inhibition

The zones of inhibition assays were performed to test the antimicrobial efficacy of each individual compound (n = 24). One hundred microliters of prepared cell suspension was pipetted and spread across the surface of the agar. Three equal wells (8 mm diameter) were cut out of the each agar plates. To each of the wells, 100 µL of suspended compound was added. The plates were incubated in the appropriate air conditions and temperature for 24 h. Following incubation, the zones of inhibition was measured in mm from four sides of each well to determine an average mean value (n = 24).

2.2.4 Minimum inhibitory concentrations (MIC)

The minimal inhibitory concentration (MIC) is defined as the lowest concentration of antimicrobial to prevent bacterial growth (Russel and Chopra, 1990). One millilitre of triphenyl tetrazolium chloride (TTC) blue metabolic dye (Sigma-Aldrich, UK), was added into 9 mL of the cell suspension so that the working concentration of the dye was 0.15 % w/v. To determine the MIC, the samples and bacteria were added to a 96 well flat-bottomed microtiter plate (MTP) and a serial dilution method used across the plate. A bacterial suspension without any compound (positive control) and un-inoculated broth (negative control) was included. After incubation, the MIC was taken as lowest concentration that inhibited the visible growth of the bacteria by comparison with the controls. Growth was indicated by a change of colour in the well to dark blue / purple.

2.3.5 Minimum Bactericidal Concentration (MBC)

The MBC is defined as the lowest concentration required to completely inactivate the inoculum at a given time (Humphreys et al., 2011). To perform the MBC assays, 25 µL was sampled and

pipetted onto agar plates from the MIC well that showed no growth and also from the first well that showed growth and incubated overnight in appropriate conditions. After incubation, the lowest concentration well sample that showed no growth on the agar plate was determined to be the MBC for that test sample.

2.3.6 Statistical analysis

Statistical tests were carried out using a two tailed distribution *t*-test with two sample homoscedastic variance. Results were reported as mean ± standard error or percentage and any observed differences were considered significant at a $p < 0.05$.

3. Results

3.1 Particle characterisation

In order to assess the antibacterial activity of four compounds, graphite, GO, AgGO and ZnOGO, the compounds and hybrid molecules were firstly obtained or synthesized, then characterised and then tested using well-established antibacterial assays. The XRD patterns relating to the graphite powder produced the expected characteristic diffraction peaks at 2θ = 26.6°, 44.7° and 54.6°, corresponding to the (002), (101) and (004) diffraction peaks of graphite powder respectively (Fig. 1a and a′). XRD (Fig.1 a′) plotted over a narrower 2θ range and with a finer counts scale, showed some disordered material as evidenced by the wide peak between ca. 7 and 17° and by a characteristic 'sharp' peak was evident at 2θ = 11.8° (Fig. 1b). The composition of the GO sample was confirmed as corresponding to the (002) diffraction peak of disordered GO. Application of the Bragg equation to the reflection peak angles, revealed that the interplanar distance increased from 0.35 nm in graphite to 0.75 nm in graphene oxide. For the latter, EDX gave 54.6 wt.% C and 45.3 wt.% O (O/C ratio = 0.83), whilst the former (graphite) had an oxygen content of only 8.9 wt.%, with all of the remainder being carbon (Table 1).

200 The ZnOGO was confirmed by XRD to have a high concentration of ZnO (Fig. 1c). Diffraction
201 peaks were evident at 2θ = 32.2°, 34.8°, 36.7°, 48.0°, 57.0°, 63.3°, 66.8°, 69.5° and 72.9° which
202 corresponded to the (100), (002), (101), (102), (110), (103), (112), (201) and (004) crystalline
203 planes of ZnO, respectively (Liu et al., 2012). EDX revealed that the ZnOGO contained C (8.60
204 wt.%), O (18.75 wt.%) and Zn (72.65 wt.%). Due to the low level of carbon in ZnOGO, the
205 (002) reflection for GO (centred at ca. 10°) (Fig. 1c′) was very weak. The ZnOGO was light
206 grey in colour thus confirming the presence of carbon in the sample.
207 Following analysis of the AgGO, the diffraction peaks occurred at 2q = 38.7°, 44.9°, 65.0° and
208 77.9° (Fig. 1d). These peaks corresponded to the (111), (200), (220) and (311) crystallographic
209 planes of face-centred cubic silver. A small amount of Ag_2O was present as evidenced by the
210 corresponding (110) and (111) reflections at 28.4° and 3332.8° respectively. The (002)
211 reflection of the GO was significantly attenuated (Fig. 1d) and shifted from 11.8° to 10° ($d_{(002)}$
212 = 0.86 nm). There was also a broad reflection peak over the range 12° and 18°, with two small
213 peaks centred at 15° and 20° (Fig. 1d′) whereby corresponding d values were 0.60 nm and 0.44
214 nm, respectively, indicating the presence of disordered structures.
215 Diffuse Reflectance Infrared Fourier Transform Spectroscopy (DRIFTS) was used to further
216 characterise the compounds. Overlaid DRIFTS spectra of the 4000 cm^{-1} – 2000 cm^{-1} region for
217 the graphite, GO and AgGO demonstrated that the DRIFTS spectrum of graphite (Fig. 2a) was
218 largely featureless as expected, though there was a small and negative hydrogen bonded OH
219 stretching peak which was due to there being slightly more moisture in the background than
220 the sample. The size and position of this band did not hinder interpretation of this spectral
221 region for GO or AgGO. Graphene oxide (Fig. 2b) showed the expected broad envelope of
222 hydrogen bonded OH stretching vibrations from 3700 cm^{-1} to 2500 cm^{-1}, together with some
223 OH bands at 3650 cm^{-1} that appeared to be much less involved in hydrogen bonding. Interaction
224 of the GO with the silver (Fig. 2c) appeared to remove the latter OH stretching band and

generally attenuated the hydrogen bonded OH stretching within the region above 3350 cm^{-1}. There were some small aliphatic C-H stretching vibrations at 2946 cm^{-1} (asymmetric) and 2877 cm^{-1} (symmetric). The 2000 cm^{-1} to 400 cm^{-1} region of the same three samples demonstrated that the graphite spectrum (Fig. 3a) was again featureless apart from a small negative peak at 1650 cm^{-1} which could be assigned to an O-H bend of water, indicating again that there was slightly more moisture in the background than the sample; this peak did not interfere with interpretation. The GO featured all the expected peaks (Fig. 3b); carbonyl stretching (1738 cm^{-1}); skeletal aromatic C=C vibrations (1615 cm^{-1}); C-OH stretching (1356 cm^{-1}); C-O-C stretching (1225 cm^{-1}); C-O stretching (1056 cm^{-1}); aromatic C-H bending (849 cm^{-1}). The AgGO (Fig. 3c) also featured the same absorption bands but with the following significant differences: carbonyl stretching, skeletal aromatic C=C vibrations and C-O-C stretching vibrations were all red-shifted by 10 cm^{-1}, 29 cm^{-1} and 5 cm^{-1}, respectively. Furthermore, the C-O vibration was split and consisted of a blue shifted component (1078 cm^{-1}) and a red shifted component (1037 cm^{-1}) (Table 2).

Overlaid spectra of the synthesised ZnO and ZnOGO demonstrated in both spectra, carbon dioxide absorption at 2350 cm^{-1} (Fig. 4) and carbonate absorptions at ca. 1580 cm^{-1} and 1380 cm^{-1} (Fig. 5). SEM showed that the compounds were heterogeneous and irregular in size (Table 3) and shape (Fig. 6). Graphite (Fig. 6a) had a flattened, irregular, random orientation, fractured, sheet like morphology with sharp, cleaved edges (0.10 μm – 25.7 μm). Graphene oxide (Fig. 6b) was composed of aggregated creased platelets (0.20 μm – 20.0 μm). The ZnOGO (Fig. 6c) consisted of numerous aggregated nanoparticles and / or nanoparticles covering micron-sized particles (0.05 μm – 30.0 μm). AgGO (Fig. 6d) was similar to GO in appearance; creased aggregated platelets with a random scattering of nanoparticles (possibly silver and / or silver oxide) (0.01 μm- 13.0 μm).

3.2 Microbiological analysis

Zones of inhibition assays were carried out against Gram-negative *E. coli* and *K. pneumoniae* and Gram-positive *S. aureus* and *Enterococcus faecium* (Fig. **7**). Following the zone of inhibition assays, all the compounds demonstrated antimicrobial activity against *E. coli* and all the GO-containing compounds demonstrated antimicrobial activity against *S. aureus*. Graphite was only effective against *E. coli* and thus demonstrated a significantly greater antimicrobial efficacy than GO or ZnOGO against this bacteria ($p > 0.05$). The most effective antimicrobial overall against the bacteria using zones of inhibition was AgGO which provided the greatest zones of inhibition against *E. coli* (4.48 mm) and *S. aureus* (4.50 mm).

The MIC results demonstrated that against *E. coli* all the compounds were effective at concentrations of 0.125 mg mL^{-1}. Against *S. aureus,* graphene oxide was the most effective (0.125 mg mL^{-1}) whilst AgGO was the most effective against *Enterococcus faecium* (0.125 mg mL^{-1}). *K. pneumoniae* was again the most difficult bacteria to inhibit. However, the ZnOGO and AgGO compounds demonstrated statistically significant inhibitory effects compared to the graphite and GO compounds against *K. pneumoniae* at concentrations of 0.25 mg mL^{-1} ($p > 0.05$). MBCs demonstrated that against *E. coli,* ZnOGO and AgGO were the most effective at 0.125 mg mL^{-1}. GO, ZnOGO and AgGO were all effective against *S. aureus* at a concentration of 0.25 mg mL^{-1} whilst AgGO was the most effective against *Enterococcus faecium* (0.125 mg mL^{-1}) (Fig. 8b). It was demonstrated that as with the other assays, *K. pneumonia* was the most difficult bacteria to eradicate, demonstrating the greatest MBC values. However, AgGO was the most effective hybrid compound against this bacteria at a concentration of 0.25 mg mL^{-1}.

4. Discussion

4.1 Characterisation of compounds

The XRD patterns relating to the graphite powder produced the expected characteristic diffraction peaks (Peng et al., 2013). The composition of the GO sample was confirmed (Chowdhuri et al., 2015) and it was evident that the (002) reflection had shifted to a lower

angle and was of much lower intensity, relative to the same reflection in graphite. These observations are well established and indicate the formation of pendent oxygen containing functional groups on the top and bottom surfaces of the basal planes that increase the interplanar distance; this resulted in the shift of the (002) reflection to a lower angle demonstrating significantly decreased stacking uniformity (resulting in reduced reflection intensity). This is consistent with the DRIFTS data that indicated prolific functionalisation. The XRD also demonstrated disruption of the relatively ordered stacking of GO platelets due to non-uniform intercalation by the ZnO nanoparticles and / or coverage of the ZnO particles by GO, which may have contributed to a reduced intensity of the reflection (Chowdhuri et al., 2015). The AgGO peaks corresponded to crystallographic planes of face-centred cubic silver (Zhou et al., 2007). A small amount of Ag_2O was present but as the atomic radius of silver is 0.17 nm, it is conceivable that individual silver atoms may have intercalated the platelets (Dhoondia and Chakraborty, 2012). The attenuation of the (002) reflection indicated that the otherwise relatively regular stacking of GO had probably been disrupted by non-uniformly sized Ag nanoparticles between the GO platelets. It is also plausible that the GO may form a coating on the Ag nanoparticles (Oo, 2007; Das et al., 2011; Ma et al., 2011). The level of silver (by EDX) in the sample was 57.9 wt.%; a mix of GO intercalation by Ag nanoparticles and GO coating of Ag nanoparticles may therefore be likely. The level of carbon (20.3 wt.%) can be accommodated by the proposed structures of the hybrid. The oxygen in the Ag_2O will have contributed to the amount of overall oxygen identified in the sample (21.8 wt %).

The DRIFTS spectrum of graphite was largely featureless as expected. GO showed the expected broad envelope of hydrogen bonded OH stretching vibrations. AgGO appeared to remove the latter OH stretching band and generally attenuated the hydrogen bonded OH stretching. This may be due to the interaction of the silver with weakly hydrogen bonded OH groups (phenolic OH and other OH) of the GO. The more general attenuation of the hydrogen

bonded O-H bands, within the region above 3350 cm^{-1}, may be related to reduced water content in the AgGO and / or interaction of the silver with the hydrogen bonded OH groups of the GO. There were some small aliphatic C-H stretching vibrations. These may be due to residual ethylene glycol from the compound synthesis and to a lesser extent, residual ethanol from washing. The C-O vibration was split and consisted of a blue shifted component (1078 cm^{-1}) and a red shifted component (1037 cm^{-1}). These observations indicated a significant interaction of the GO platelets with the silver. The latter is further supported by a blue shift in the aromatic C-H bending and C-OH stretching band. Interaction of the silver with carbonyl species and with the residual *p*-electrons in the GO would lead to the observed red shifts as the bond vibration was damped by interaction with the electron orbitals of silver atoms. This would also result in shortening of the aromatic C-H bonds and phenolic and carboxylic acid C-OH bonds, hence giving rise to the observed blue shift. The split in the C-O vibration indicated silver interactions having varying effects on the different ether linkages in the GO. It may be speculated that the ether groups at the platelet edges would be blue shifted and those actually pendant from a platelet surface may be red-shifted due to their interaction with the silver atoms. These observations are supported by the XRD data which indicated that the usual relatively ordered structure of the GO had been destroyed by its interaction with the silver. It may be that the silver atoms / particles had intercalated the layers resulting in highly non-uniform stacking. This would lead to the significantly attenuated and broadened GO related reflections in the XRD data for the AgGO.

The features observed using the DRIFTS analysis were expected in the ZnO that had been synthesised via this route since the carbonate and carbon dioxide would be decomposition products of the starting materials (Selim et al., 2015). The carbonate would have been converted to CO_2 as the annealing temperature increased, resulting in the CO_2 becoming trapped within the structure. Interestingly, the OH stretching bands were more intense in the

ZnOGO, and it may be that these were related to the GO, though the associated carbonyl and C-O bands could not be resolved. This may be explained by the strong association between the GO and ZnO resulting in attenuation of these vibrations. The GO may have coated the surface of the synthesised ZnO particles and / or could have become interleaved within the synthesised ZnO structures. In either case, the relatively ordered stacking of the GO platelets had become disrupted. The XRD data supports the latter proposition. The other area of interest in these spectra was the Zn-O bending vibrations at ca. 440 and 520 cm^{-1}. In the ZnOGO, the ZnO band at 520 cm^{-1} was stronger than in the synthesised ZnO (Fig. 5b). To the authors knowledge, such observations have not been reported elsewhere, but it may be related to a difference in the chemical environment and possibly due to the interactions with the GO.

SEM demonstrated that the compounds were heterogeneous and irregular in size and shape. The ZnOGO particles had the greatest size range (0.05 μm – 30 μm), whereas AgGO and ZnOGO had the smallest sized particles (0.01 μm and 0.05 μm respectively) demonstrating the availability of both nano- and micron sized particles.

4.2 Microbiology

The zone of inhibition assays demonstrated that none of the compounds had any effect against *Enterococcus faecium* or *K. pneumoniae*. This may be due to the zone of inhibition method being carried out using a semi-solid media; this combined with the thick capsule of the *K. pneumoniae* and the insusceptible nature of the *Enterococcus faecium* may have resulted in the reduced antimicrobial effect demonstrated. Further, the bacteria in this method were growing on the agar in colonies. These ‘communities’ of bacteria may have been more resistant to the antimicrobial effects of the compounds, similar to the effects observed when bacteria form biofilms (Gilbert et al., 2002) rather than what was observed when the bacteria are in planktonic form as in the MIC and MBC.

Work by others has demonstrated the antibacterial activities of graphite and graphite oxide towards *E. coli* and it was found that a GO dispersion demonstrated an 89.7% of loss viability at 40 mg mL^{-1} (Liu et al., 2007). In our work, we demonstrated an antimicrobial activity of GO at much lower concentrations against the four bacterial strains tested (MIC = 0.125 mg mL^{-1} – 0.5 mg mL^{-1}; MBC = 0.25 mg mL^{-1} – 0.5 mg mL^{-1}). Work by Xie et al. (2011) demonstrated the MIC of ZnO nanoparticles for *Escherichia coli* O157:H7 was found to be 0.4 mg mL^{-1}. In comparison with our work, ZnOGO was the most antimicrobial compound against *E. coli* with an MIC at the lower concentration of 0.125 mg mL^{-1}. However, the *E.coli* used in our study was a different strain. The ZnOGO was also inhibitory against *S. aureus, Enterococcus faecium* and *K. pneumoniae* at a MIC of 0.25 mg mL^{-1}. GO and AgGO were also effective against *S. aureus* and *Enterococcus faecium* at concentrations of 0.125 mg mL^{-1}. Work by others also demonstrated that the MIC for ZnO nanoparticles was 1.5 mg mL^{-1} and 3.1 mg mL^{-1} against *S. aureus* and *E. coli* respectively demonstrating that in some cases our ZnOGO compound was more effective than the antimicrobial action of ZnO alone used in other studies (Franklin et al., 2007; Azam et al., 2012). The MIC against *Enterococcus faecium* and *K. pneumoniae* was optimal with the AgGO hybrid compound. ZnOGO also demonstrated the same MIC as AgGO against *K. pneumoniae.*

Results from the MBC assays demonstrated that *K. pneumonia* was the most difficult bacteria to eradicate. Work by others using MBC assays with 18 nm nanoparticles of ZnO demonstrated that the concentration of particles required against *E. coli* was 0.018 mg mL^{-1} and 0.016 mg mL^{-1} against *S. aureus* (Xie et al., 2011). However, in contrast with their results, our compounds required greater concentrations in order to obtain the MBC. This may be explained by the particle size of our compounds being generally larger. It has been suggested that the smaller the size of the compounds, the greater the antimicrobial activity of the agent, however

373 contradictory results have been reported where size dependent effects were not found to
374 influence the antimicrobial activity of ZnO (Chen et al., 2014).
375 The antimicrobial activity of the hybrid compounds may be explained in part by either the
376 shape of the compound particles or by the percent of active facets. The atomic structure of the
377 particle surface will affect its interaction with the bacterial cells (Selim et al., 2015). It is
378 expected that the adsorption of atoms and molecules as a result of the interaction of the particles
379 with the environment will be altered on the different planes, thus the difference in the atomic
380 structure of the particles may result in a difference in their surface properties that could affect
381 their interaction with the bacteria, leading to different antimicrobial efficacies (Pal et al., 2007).
382 It has been suggested that high density facets with (111) faces exhibit greater amounts of
383 antimicrobial activity (Pal et al., 2007). This is in agreement with our work since the AgGO
384 demonstrated the greatest numbers of (111) planes. Combined with the shape of the
385 compounds, these crystal structures can influence their mechanism of bacterial internalisation
386 of the cell wall (Sirelkhatim et al., 2015).
387 Work by Liu et al. (2011) focused on the interactions of GO and graphite on bacterial
388 membranes against *Escherichia coli*. In agreement with our results, they showed that a GO
389 dispersion had a greater amount on antibacterial activity than graphite. GO and graphite are
390 thought to confer antimicrobial activity due to membrane stress on the bacterial cells induced
391 by the sharp edges of the compounds (Liu et al., 2011; Chen et al., 2014). An interesting fact
392 that was evidenced in this work was that the type of antimicrobial assay used produced a range
393 of results and thus it may be concluded that the use of one antimicrobial assay to determine the
394 efficacy of compounds is not sufficient. Further, the type of antimicrobial assay used should be
395 selected in line with the proposed final application of the antimicrobials.
396 Following each of the antimicrobial tests, AgGO demonstrated the greatest overall
397 antimicrobial efficacies. *E. coli* was the most susceptible to the compounds followed by *S.*

aureus, Enterococcus faecium and finally *K. pneumoniae.* This can be explained in part by the nature of the microorganisms physiology. The Gram-negative microorganisms *E. coli* and *K. pneumoniae* are surrounded by an outer and inner cell membrane which have between them a thin layer of peptidoglycan. However, *K. pneumoniae* also has a large polysaccharide capsule surrounding the bacterial cell; in addition, this capsule acts as a barrier to antimicrobial agents (Highsmith and Jarvis, 1985). *S. aureus* and *Enterococcus faecium* are Gram-positive bacteria that have a cell membrane, chiefly composed of thick peptidoglycan. However, Enterococci are intrinsically more resistant to many antibiotics since unlike acquired resistance and virulence traits which are usually encoded by plasmids or transposon elements, their intrinsic resistance is based on chromosomal genes (Huycke et al., 1998). Further, a number of antibiotics demonstrate bacteriostatic but not bactericidal activity against *Enterococcus faecium* bacteria (Huycke et al., 1998). Thus, the use of AgGO against these two resilient bacteria may be an important step in maintaining the hygienic status of areas into which the molecule is applied or incorporated.

5. Conclusions

ZnOGO and AgGO hybrid compounds were successfully produced and characterised. AgGO was the most effective antimicrobial and enhanced the activity of GO. The effect of the compounds on the bacteria did not relate to the Gram-positive or Gram-negative structures of the bacteria but rather, was due to their microorganisms overall physiology. GO-metal hybrids have the potential to be beneficially utilised as novel antimicrobials or biocides in settings where bacteria are becoming increasingly problematic.

Acknowledgements

The authors would like to acknowledge that the work was funded by Manchester Metropolitan University. P. Ramalingam would also like to acknowledge a Newton-Bhabha fellowship from the British Council.

References

Anandan, S., Muthukumaran, S., 2015. Microstructural, crystallographic and optical characterizations of Cu-doped ZnO nanoparticles co-doped with Ni. Journal of Materials Science: Materials in Electronics 26, 4298-4307.

Azam, A., Ahmed, A. S., Oves, M., Khan, M. S., Habib, S. S., Memic, A., 2012. Antimicrobial activity of metal oxide nanoparticles against Gram-positive and Gram-negative bacteria: A comparative study. International Journal of Nanomedicine 7, 6003-6009.

Boucher, H. W., Talbot, G. H., Bradley, J. S., Edwards, J. E., Gilbert, D., Rice, L. B., Scheld, M., Spellberg, B., Bartlett, J., 2009. Bad Bugs, No Drugs: No ESKAPE! An Update from the Infectious Diseases Society of America. Clinical Infectious Diseases 48, 1-12.

Chaturvedi, A., Bajpai, A.K., Bajpai, J., Singh, S.K., 2016. Evaluation of poly (vinyl alcohol) based cryogel-zinc oxide nanocomposites for possible applications as wound dressing materials. Materials Science & Engineering C-Materials for Biological Applications 65, 408-418.

Chen, J., Peng, H., Wang, X., Shao, F., Yuan, Z., Han, H., 2014. Graphene oxide exhibits broad-spectrum antimicrobial activity against bacterial phytopathogens and fungal conidia by intertwining and membrane perturbation. Nanoscale 6, 1879-1889.

Chowdhuri, A. R., Tripathy, S., Chandra, S., Roy, S., Sahu, S. K., 2015. A ZnO decorated chitosan–graphene oxide nanocomposite shows significantly enhanced antimicrobial activity with ROS generation. RSC Advances 5, 49420-49428.

Das, M. R., Sarma, R. K., Saikia, R., Kale, V. S., Shelke, M. V., Sengupta, P., 2011. Synthesis of silver nanoparticles in an aqueous suspension of graphene oxide sheets and its antimicrobial activity. Colloids and Surfaces B: Biointerfaces 83, 16-22.

446 Deokar, A.R., Shalom, Y., Perelshtein, I., Perkas, N., Gedanken, A., Banin, E., 2016. A
447 topical antibacterial ointment made of Zn-doped copper oxide nanocomposite. Journal of
448 Nanoparticle Research 18, 1-6.
449 Dhoondia, Z. H., Chakraborty, H., 2012. Lactobacillus Mediated Synthesis of Silver Oxide
450 Nanoparticles. Nanomaterials and Nanotechnology 2, 15.

451 Franklin, N. M., Rogers, N. J., Apte, S. C., Batley, G. E., Gadd, G. E., Casey, P. S., 2007.
452 Comparative toxicity of nanoparticulate ZnO, bulk ZnO, and ZnCl2 to a freshwater microalga
453 (Pseudokirchneriella subcapitata): the importance of particle solubility. Environtmenal Science
454 and Technology 41, 8484-8490.

455 Gilbert, P., Allison, D. G., McBain, A. J., 2002. Biofilms in vitro and in vivo: do singular
456 mechanisms imply cross-resistance? Journal of Applied Microbiology 92, 98s-110s.

457 Highsmith, A. K., Jarvis, W. R., 1985. Klebsiella pneumoniae: selected virulence factors that
458 contribute to pathogenicity. Infection Control 6, 75-77.

459 Hummers Jr, W. S., Offeman, R. E., 1958. Preparation of graphitic oxide. Journal of the
460 American Chemical Society 80, 1339-1339.

461 Humphreys, G., Lee, G. L., Percival, S. L., McBain, A. J., 2011. Combinatorial activities of
462 ionic silver and sodium hexametaphosphate against microorganisms associated with chronic
463 wounds. Journal of Antimicrobial Chemotherapy 66, 2556-2561.

464 Huycke, M. M., Sahm, D. F., Gilmore, M. S., 1998. Multiple-drug resistant enterococci: the
465 nature of the problem and an agenda for the future. Emerging Infectious Diseases 4, 239-249.

466 Jennings, M. C., Minbiole, K. P., Wuest, W. M., 2015. Quaternary Ammonium Compounds:
467 An Antimicrobial Mainstay and Platform for Innovation to Address Bacterial Resistance. ACS
468 Infectious Diseases 1, 288-303.

469 Kumar, S. S., Venkateswarlu, P., Rao, V. R., Rao, G. N., 2013. Synthesis, characterization and
470 optical properties of zinc oxide nanoparticles. International Nano Letters 3, 30.

471 Li, Z. Q., Lu, C. J., Xia, Z. P., Zhou, Y., Luo, Z., 2007. X-ray diffraction patterns of graphite
472 and turbostratic carbon. Carbon 45, 1686-1695.

473 Liauw, C. M., 2003. Particulate Filled Composites (2nd Edition), Ed. Rothon RN, Smithers
474 RAPRA technology.

475 Liu, H., Zhang, Y., Yang, H., Xiao, W., Sun, L., 2016. Filter Paper Inspired Zinc Oxide
476 Nanomaterials with High Photocatalytic Activity for Degradation of Methylene Orange.
477 Journal of Chemistry 2016, 1-7.

478 Liu, L. F., Barford, J., Yeung, K. L., Si, G., 2007. Non-UV based germicidal activity of metal-
479 doped TiO2 coating on solid surfaces. Journal of Environmental Science (China) 19, 745-750.

480 Liu, Q., Yao, X., Zhou, X., Qin, Z., Liu, Z., 2012. Varistor effect in Ag–graphene/epoxy resin
481 nanocomposites. Scripta Materialia 66, 113-116.

482 Liu, S., Zeng, T. H., Hofmann, M., Burcombe, E., Wei, J., Jiang, R., Kong, J., Chen, Y., 2011.
483 Antibacterial activity of graphite, graphite oxide, graphene oxide, and reduced graphene oxide:
484 membrane and oxidative stress. ACS Nano. 5, 6971-6980.

485 Ma, J., Zhang, J., Xiong, Z., Yong, Y., Zhao, X. S., 2011. Preparation, characterization and
486 antibacterial properties of silver-modified graphene oxide. Journal of Materials Chemistry 21,
487 3350-3352.

488 Oo, H. W. M., 2007. Infrared Spectroscopy of Zinc Oxide and Magnesium Nanostructures.
489 Ph.D Thesis. Washington State University.

Pal, S., Tak, Y. K., Song, J. M., 2007. Does the Antibacterial Activity of Silver Nanoparticles Depend on the Shape of the Nanoparticle? A Study of the Gram-Negative Bacterium Escherichia coli. Applied and Environmental Microbiology 73, 1712-1720.

Peng, S. G., Fan, X. J., Li, S., Zhang, J., 2013. Green synthesis and characterization of graphite oxide by orthogonal experiment. Journal of the Chilean Chemical Society 58, 2213-2217.

Russel, A. D., Chopra, I., 1990. Understanding antimicrobial resistance and action. Ellis Horwood, Chichester.

Selim, M. S., El-Safty, S. A., El-Sockary, M. A., Hashem, A. I., Abo Elenien, O. M., El-Saeed, A. M., Fatthallah, N. A., 2015. Modeling of spherical silver nanoparticles in silicone-based nanocomposites for marine antifouling. RSC Advances 5, 63175-63185.

Sirelkhatim, A., Mahmud, S., Seeni, A., Kaus, N. H. M., Ann, L. C., Bakhori, S. K. M., Hasan, H., Mohamad, D., 2015. Review on Zinc Oxide Nanoparticles: Antibacterial Activity and Toxicity Mechanism. Nano-Micro Letters 7, 219-242.

Tayel, A. A., El-Tras, W. F., Moussa, S., El-Baz, A. F., Mahrous, H., Salem, M. F., Brimer, L., 2011. Antibacterial action of zinc oxide nanoparticles against foodborne pathogens. Journal of Food Safety 31, 211-218.

Velmurugan, P., Park, J.H., Lee, S.M., Yi, Y.J., Cho, M., Jang, J.S., Myung, H., Bang, K.S., Oh, B.T., 2016. Eco-friendly approach towards green synthesis of zinc oxide nanocrystals and its potential applications. Artificial Cells Nanomedicine and Biotechnology 44, 1537-1543.

Unwin, P.R., Guell, A.G., Zhang, G.H., 2016. Nanoscale Electrochemistry of sp(2) Carbon Materials: From Graphite and Graphene to Carbon Nanotubes. Accounts of Chemical Research 49, 2041-2048.

513 Wang, D., An, J., Luo, Q., Li, X., Yan., L 2012. Nano Antimicrobials. Springer, London
514 New York.
515 Xie, Y., He, Y., Irwin, P. L., Jin, T., Shi, X., 2011. Antibacterial activity and mechanism of
516 action of zinc oxide nanoparticles against *Campylobacter jejuni*. Applied of Environmental
517 Microbiology 77, 2325-2331.
518 Zhou, J., Zhao, F., Wang, Y., Zhang, Y., Yang, L., 2007. Size-controlled synthesis of ZnO
519 nanoparticles and their photoluminescence properties. Journal of Luminescence 122, 195-197.
520

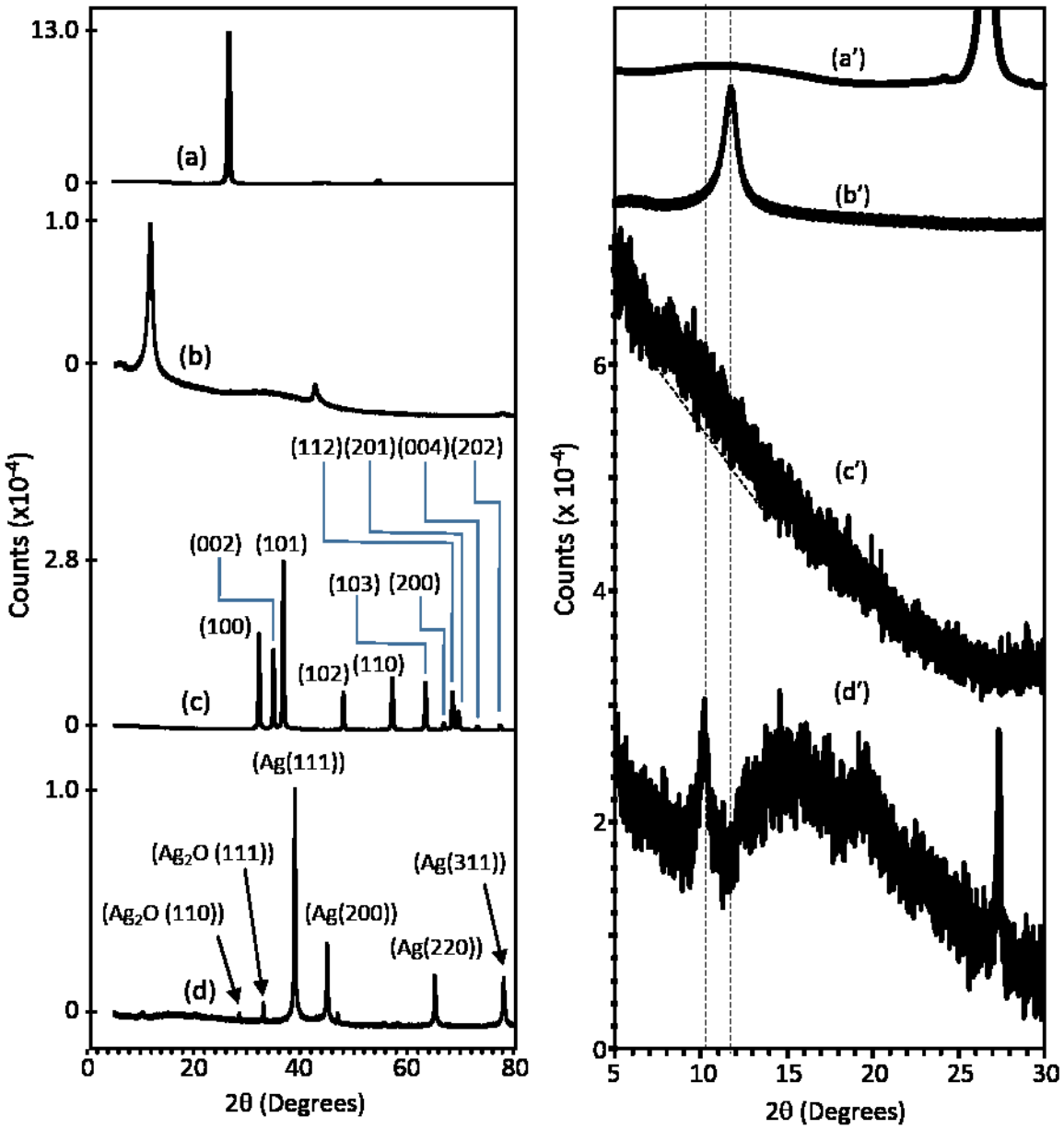

521

522 **Fig. 1** X-Ray Diffraction patterns for; (a) graphite, (b) graphene oxide (GO), (c) zinc oxide – graphene
523 oxide hybrid (ZnOGO) and (d) silver – graphene oxide hybrid (AgGO). Note the individual peak heights
524 – patterns have been compressed to fit. In the right hand stack, patterns a' to d' correspond to those
525 in the left stack but are plotted over a narrower 2q range on common counts scale (with Y-shifting for
526 presentation purposes). ZnOGO and AgGO have 50 x boosted counts and are Y-shifted for presentation
527 purposes.

528

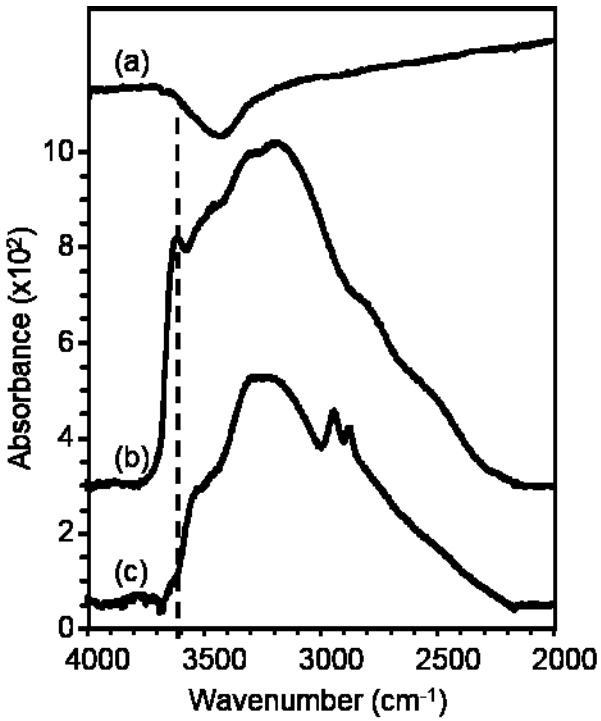

529

530 **Fig. 2** DRIFTS spectra (4000 cm^{-1} to 2000 cm^{-1}) of (a) graphite, (b) graphene oxide (GO) and (c) silver –
531 graphene oxide hybrid (AgGO).

532

533

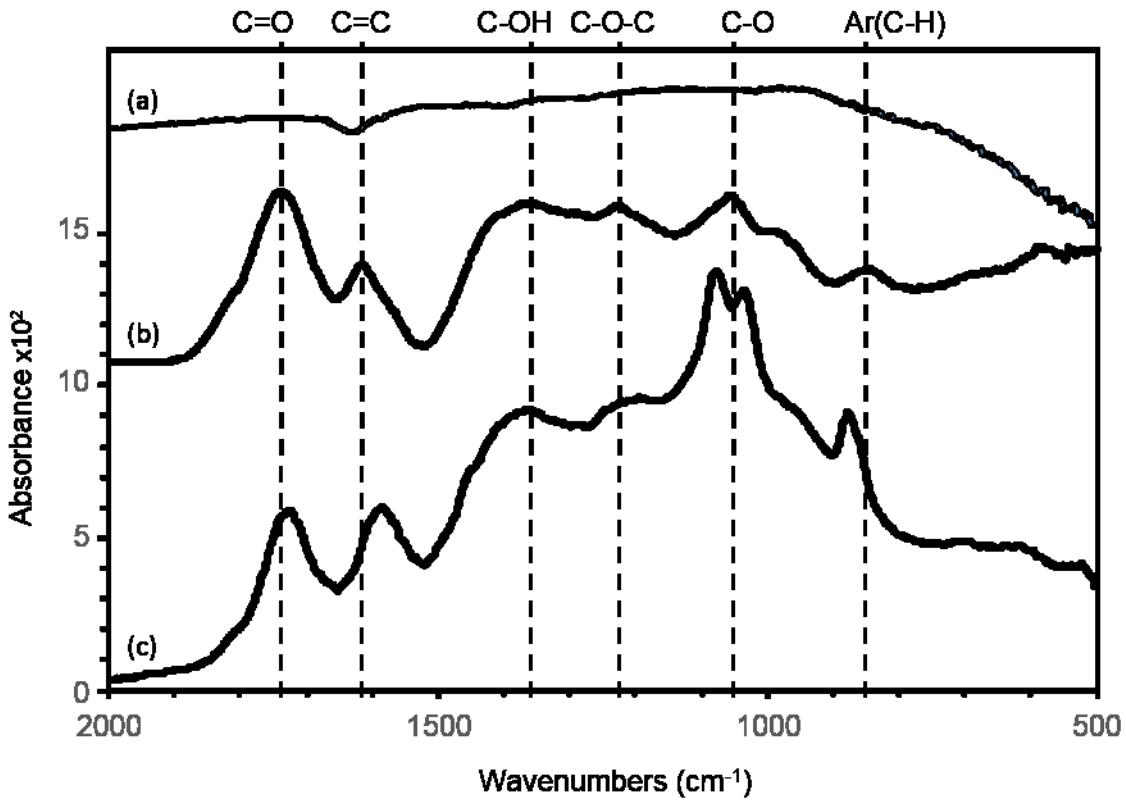

534

535 **Fig. 3** DRIFTS spectra (2000 cm^{-1} to 500 cm^{-1}) of (a) graphite, (b) graphene oxide (GO) and (c) silver –
536 graphene oxide hybrid (AgGO).

537

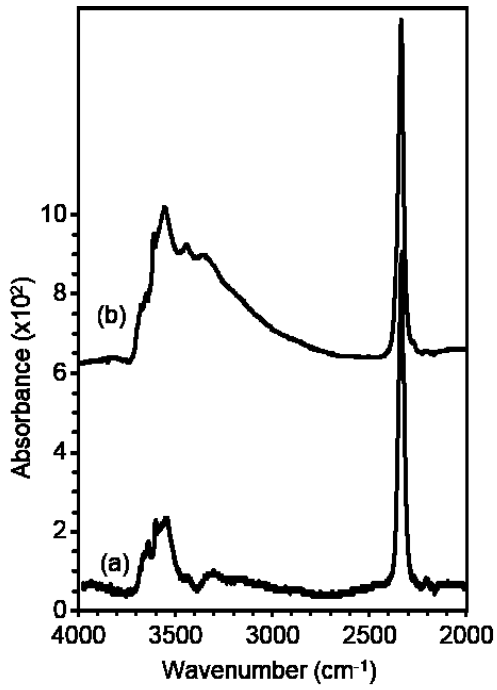

538

539 **Fig. 4** DRIFTS spectra (4000 cm^{-1} to 2000 cm^{-1}) of (a) synthesised zinc oxide (ZnO), (b) synthesised zinc
540 oxide – graphene oxide hybrid (ZnOGO).

541

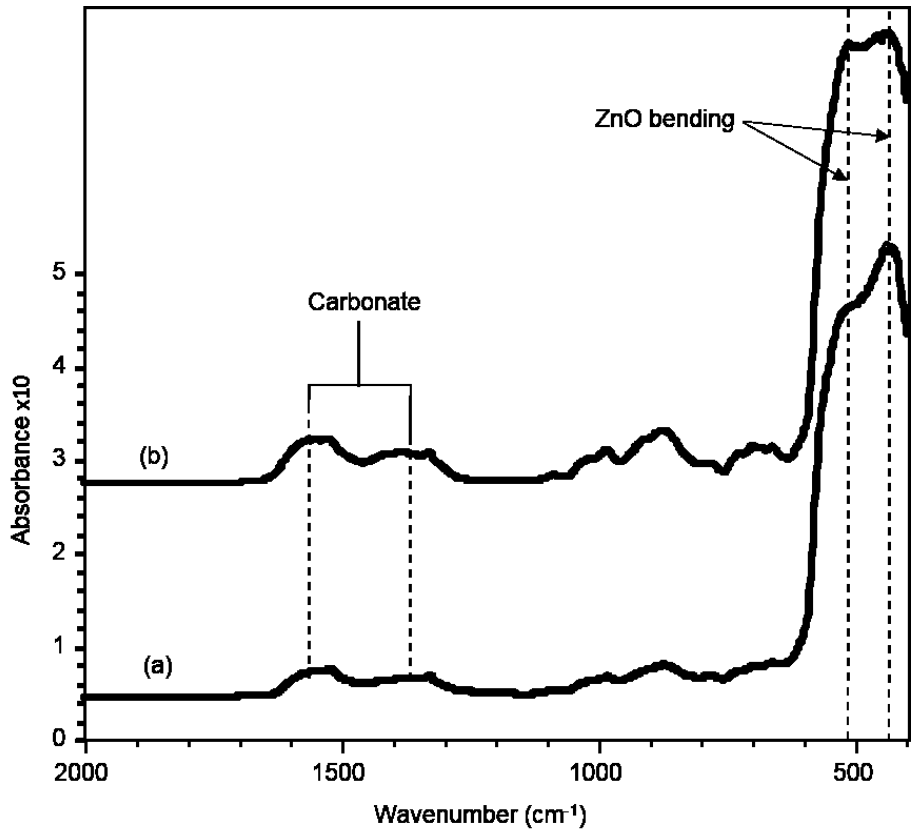

542

543 **Fig. 5** DRIFTS spectra (2000 cm^{-1} to 400 cm^{-1}) of (a) synthesised zinc oxide (ZnO), (b) synthesised zinc
544 oxide – graphene oxide hybrid (ZnOGO).

545

546

547 a) 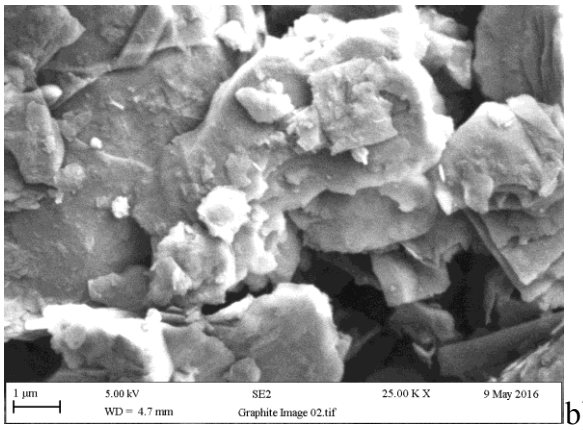

b) 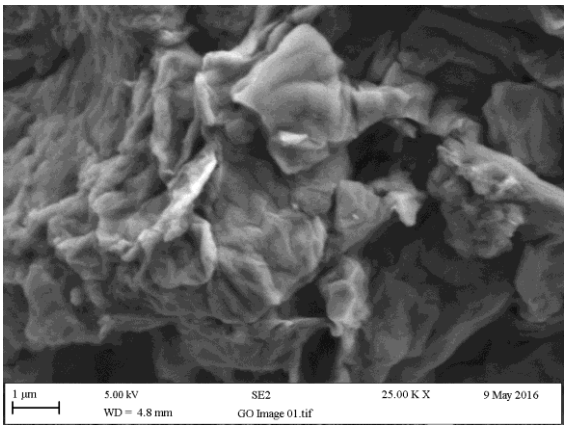

548 c) 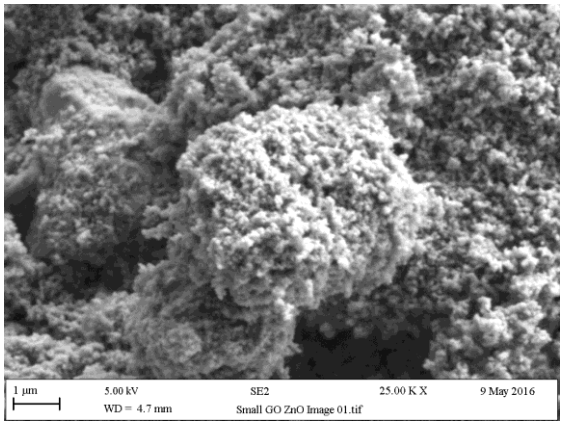

d) 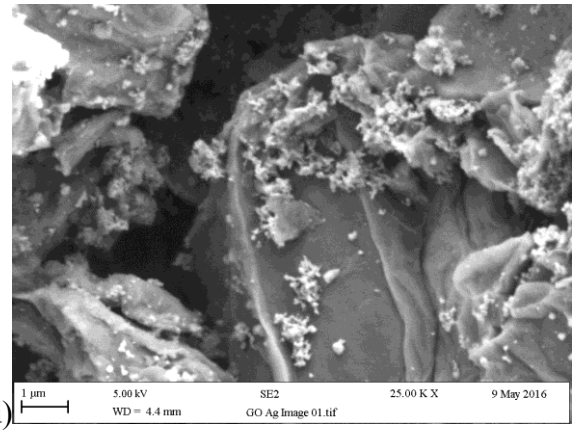

549 **Fig. 6** SEM images demonstrating the morphology and particle sizes of a) graphite, b) graphene oxide
550 (GO), c) zinc oxide – graphene oxide hybrid (ZnOGO) and d) silver – graphene oxide hybrid (AgGO).

551

552

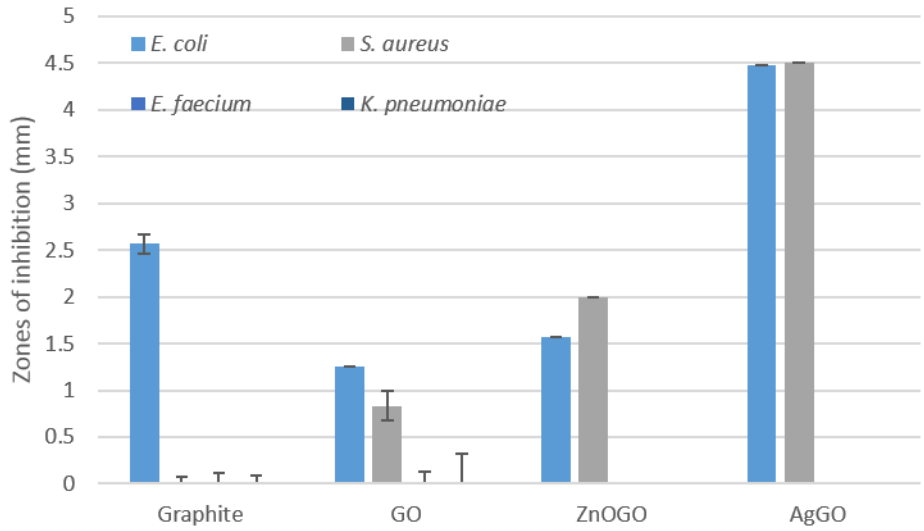

553

554 **Fig. 7** Zone of inhibition measurements demonstrating the antimicrobial efficacy of the compounds.
555 The silver – graphene oxide hybrid (AgGO) was determined to be the most effective antimicrobial
556 using this method. *K. pneumoniae* and *E. faecium* did not demonstrate inhibition by the compounds
557 using this method.

558

559

560

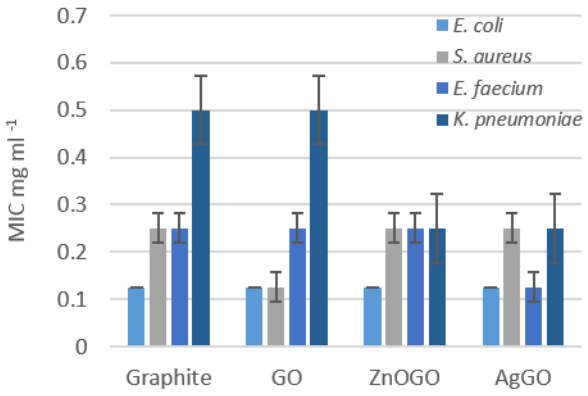

561

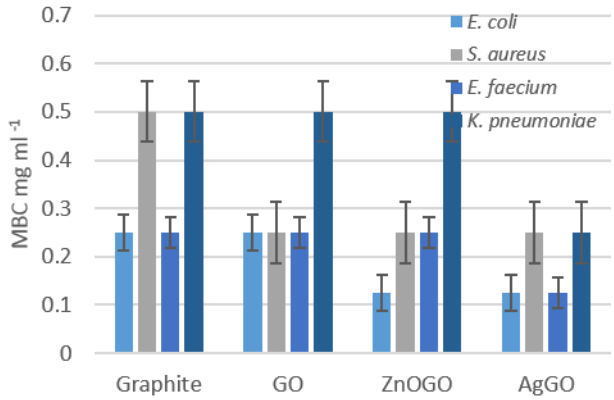

562 **Fig. 8** a) MIC and b) MBC of compounds against the four medically relevant bacteria demonstrating
563 that the silver – graphene oxide hybrid (AgGO) demonstrated the greatest inhibitory and bactericidal
564 effect.

565

566 Table 1 EDX analysis demonstrating the elemental analysis (% weight) of the compounds

	C	**O**	**Ag**	**Zn**
Graphite	91.12 ± 0.13	8.88 ± 0.13	N/A	N/A
GO	54.15 ± 0.79	45.85 ± 0.79	N/A	N/A
ZnOGO	8.60 ± 0.04	18.75 ± 0.17	N/A	72.65 ± 0.13
AgGO	14.50 ± 1.50	15.74 ± 1.03	69.77 ± 2.53	N/A

567 N/A Not applicable for elemental analysis

568

569

570 Table 2 Effect of silver addition on infrared absorption frequencies

Group vibration		Vibration frequency (cm^{-1})		Dn (cm^{-1})
		GO	Ag-GO	
C=O	1738	1728		-10
C=C	1615	1586		-29
C-OH	1356	1363		+7
C-O-C	1225	1220		-5
C-O	1056	1078		+22
		1037		-19
Aromatic C-H	849	879		+30

571

572

573 Table 3 Minimum to maximum size range of the particles

574

	Smallest size (μm)	Greatest size (μm)
Graphite	0.10	25.7
Graphene oxide	0.20	20.0
ZnOGO	0.05	30.0
AgGO	0.01	13.0

575

576

577